OPTOELECTRONICS AND ADVANCED MATERIALS-RAPID COMMUNICATIONS Vol 4, No. 6, June 2010, p. 816 - 820

Variation tendencies of tensile constrained recovery behaviour and associated structural changes during thermal cycling of a Fe-Mn-Si-Cr-Ni shape memory alloy

C. LOHAN, B. PRICOP, R. I. COMĂNECI, N. CIMPOEŞU, L.-G. BUJOREANU*
The "Gh. Asachi" Technical University from Iaşi, Bd. D. Mangeron 67, 700050 Iaşi, Romania

By means of tensile stress variation during heating-cooling, applied in each consecutive cycle, performed up to progressively higher strains, the constrained recovery behaviour of a Fe-15.8 Mn-3.8 Si-12.3 Cr-4.7 Ni (mass. %) shape memory alloy (SMA) was reported. During each cycle, temperature was increased from room temperature up to 453 K and decreased to room temperature, while keeping the specimen to a constant strain. The variation tendencies of tensile stress, developed during heating-cooling, with increasing both the number of cycles and the constant strain applied per each cycle, was evaluated and corroborated with structural changes. These changes were related to the occurrence of stress-induced martensite the relief variations of which were revealed, as well, at structural and sub-structural level.

(Received April 01, 2010; accepted June 16, 2010)

Keywords: Fe-Mn-Si-Cr-Ni shape memory alloys, Tensile constrained recovery, Thermal cycling, Stress-induced martensite, Substructure relief

1. Introduction

Shape Memory Effect (SME) in alloys represents the unique and spontaneous recovery of a "hot shape" as an effect of heating a Shape Memory Alloy (SMA) to which a "cold shape" has been previously induced. The hot shape is characteristic to parent phase (austenite) domain while the cold shape is associated with the formation of stable stress-induced martensite. The main types of SME are illustrated in Fig.1, in the case of tension loading.

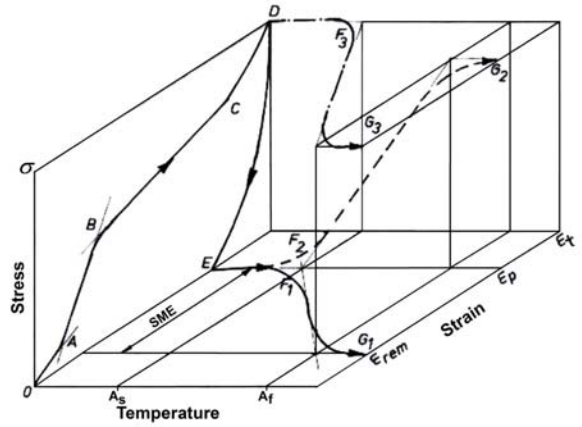

Fig.1 Illustration of the main types of tensile SME in the stress-strain-temperature space. See text for details

The tensile loading (OABCD)-unloading (DE) curve illustrates the typical behaviour of a SMA in the martensitic domain ($T < A_s$). Considering "hot shape" as undeformed (unstretched), it corresponds to point O, while "cold shape" corresponds to point E, characterized by permanent strain ε_p, where stress induced martensite is stable. During heating, up to a temperature $T > A_f$, stress induced martensite reverts to parent phase (austenite) and hot shape is partially recovered by SME, a remanent strain ε_{rem} being obtained. As a function of the conditions in which hot shape recovery occurs, one can define: (i) free recovery SME (EF_1G_1), when the output is motion; (ii) constrained recovery SME (EF_2G_2), when the output is stress and (iii) work generating SME (DF_3G_3), when the output is energy [1].

The present approach is focussed on constrained recovery SME, quantified by means of the tensile stress developed by an SM element which is prevented to recover its hot shape during heating [2]. In order to quantify the variation tendencies of tensile constrained recovery SME during thermal cycling, a Fe-Mn-Si-Cr-Ni SMA will be employed since the most successful applications of Fe-Mn-Si based SMAs are exploiting this phenomenon, being materialized as pipe joints [3], fishplates for crane rail connections [4] and brick-pre stressing rods [5].

Due to the possibility to develop rather elevated recovery stresses by constrained recovery, the phenomenon was carefully studied in various types of Fe-Mn-Si SMAs. Thus, in Fe-15Mn-5Si-9Cr-5Ni-(0.5-1.5) NbC (herein after all chemical compositions are in mass. %) recovery stresses as high as 274 MPa were reported at room temperature (RT), after a heating-cooling cycle [6] and a stress peak estimated to 240 MPa was recorded in Fe-14Mn-6Si-9Cr-5Ni during cooling from 623 K [7]. The maximum recovery stress developed in Fe-29Mn-7 Si at 773 K reached 169 MPa [8] while in the case of a Fe-23.3Mn-2.8Si SMA the maximum value was 280 MPa and was obtained at RT after two complex cycles comprising RT loading-partial unloading and heating-cooling cycles at

constant strain with additional straining between cycles [9].

Considering that: (i) in Fe-Mn-Si-Cr-Ni SMAs, the reversion of stress induced martensite to austenite is strongly influenced by a series of factors, such as annealing temperature and applied permanent strain [10] and (ii) for large pre-strains, the resulting stress induced martensite is α' (body centre cubic, bcc) instead of ε (hexagonal close packed, hcp) [11], the present paper aims to reveal the variation tendencies of a specific Fe-Mn-Si-Cr-Ni SMA, when subjected to constrained recovery cycles up to increasing strains and to corroborate these changes with the formation of stress induced martensite.

2. Experimental details

A Fe-Mn-Si-Cr-Ni SMA was cast, homogenized, hot rolled and annealed as previously detailed [10]. The chemical composition, determined by spectrogravimetry was 15.75Mn-12.26Cr-3.75Si-4.69Ni-0.42Mo-0.28Cu-0.065C-0.06V-0.04Co-0.021S-0.019P balance Fe. This alloy must respect two design conditions given in Ref. [12], in order to obtain γ phase at RT:

$$Ni_{eq} > 25.5\text{-}0.8Cr_{eq} \quad (1)$$

and to avoid the formation of σ phase:

$$Ni\% \geq (Cr\%\text{-}16C\%)/17 \quad (2)$$

where

$Ni_{eq} = Ni\% + 30C\% + 0.5Mn\% = 4.69 + 30 \times 0.065 + 0.5 \times 15.75 = 14.515$ and

$Cr_{eq} = Cr\% + Mo\% + 1.5Si\% + 0.5Nb\% = 12.26 + 0.42 + 1.5 \times 3.75 = 18.305$

With the above values, the two conditions from eqs. (1) and (2) are obviously respected.

From annealed raw material, tensile specimens with gauge dimensions $(1\times4\times20)\ 10^{-3}$ m were cut by spark erosion, as shown in Fig. 2.

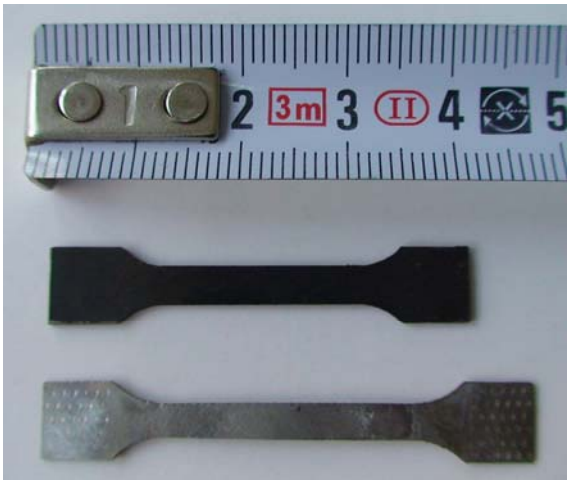

Fig. 2. Tensile specimens after spark erosion cutting (dark) and after 10 constrained recovery cycles, grinding polishing and etching.

Constrained recovery tests were performed on an INSTRON 3382 Tensile machine with thermal chamber with a deformation rate of 2.77×10^{-4}sec^{-1}. All test parameters are summarized in Table 1.

Table. 1 Summary of test parameters for tensile constrained recovery experiments.

Cycle No.	1	2	3	4	5	6	7	8	9	10
Loading time, 1.66×10^{-2} sec	3	3	3	3	3	3	3	3	3	3
Time interval	9:57 10:00	10:40 10:43	11:23 11:26	12:06 12:09	12:49 12:52	13:32 13:35	14:15 14:18	14:58 15:01	15:41 15:44	16:24 16:27
Elongation, 10^{-3} m	0.7	1.4	2.1	2.8	3.5	4.2	4.9	5.6	6.3	7.0
Heating time, 1.66×10^{-2} sec	20	20	20	20	20	20	20	20	20	20
Time interval	10:00 10:20	10:43 11:03	11:26 11:46	12:09 12:29	12:52 13:12	13:35 13:55	14:18 14:38	15:01 15:21	15:44 16:04	16:27 16:47
Heating temperature, K	453	453	453	453	453	453	453	453	453	453
Cooling time, 1.66×10^{-2} sec	20	20	20	20	20	20	20	20	20	20
Time interval	10:20 10:40	11:03 11:23	11:46 12:06	12:29 12:49	13:12 13:32	13:55 14:15	14:38 14:58	15:21 15:41	16:04 16:24	16:47 17:07
Cooling temperature	RT	RT	RT	RT	RT	RT	RT	RT	RT	RT

After testing, the elongated gauges were separated from specimens and were ground, polished and chemically treated with Villela's etchant (glycerol 45 ml + HNO3 15 ml + HCl 30 ml). Scanning electron microscopy (SEM) observations were performed on a VEGA II LSH TESCAN device, coupled with an EDX QUANTAX QX2 ROENTEC detector. The microscope is able reveal surface relief by transforming luminescence fluctuations into depths variations.

3. Experimental results and discussion

The records of the first tensile constrained recovery cycle are shown in Fig.3. Fig.3(a) displays tensile stress variation with strain during loading. Point P can be associated with yield stress located, in this case, at 400 MPa. Loading was performed on OPA, up to approx. 770 MPa corresponding to a strain of 4 %. At this strain, the mobile grip was blocked, heating was subsequently applied up to 453 K and the stress decreased along the portion ABC_1, as shown in Fig.3(b). It is noticeable that in first cycle stress decreased to zero before the end of heating. In this case, heating was interrupted in point C1, which corresponds to the start of cooling.

This behaviour corresponds to ordinary materials and has no connection to SMAs. In order to check the alloys ability to change its behaviour during "training", the number of cycles was increased. The result of applying 5

cycles is illustrated in Fig. 4.

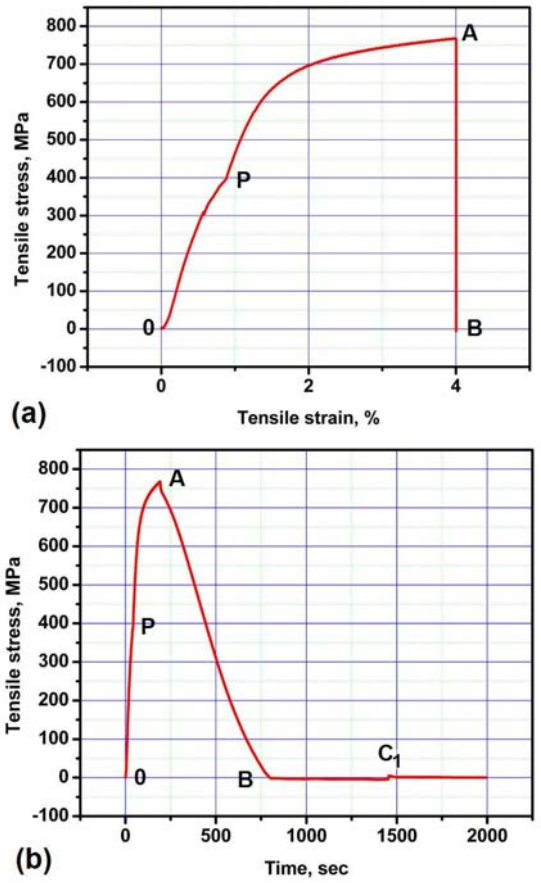

Fig. 3. First constrained recovery cycle: (a) stress-strain curve; (b) stress variation in time during the entire cycle.

It is noticeable from Fig. 4 that, after reproducing in the first cycle the variations observed in Fig.3, the increase of the number of cycles gradually induced a change of stress variations both as a function of stress and as a function of time. The first observation is that stress increased, at the end of cooling, up to point C_{1f}.

During each subsequent cycle, from the 2nd to the 5th, stress increased on loading, in Fig.4(a), from C_{if} to H_{i+1}, until reaching 800 MPa, in the fifth cycle. With increasing the number of cycles from the 1st to the 5th, the portions with constant negative stress, before and after the points C_i, become shorter and shorter. In the fifth cycle, the switching from heating to cooling occurs in a single point, C_5, located at negative stress. Moreover, in Fig.4(b) the stress-increase during cooling, between points C_i and C_{if}, becomes more and more prominent.

In order to check if the variation tendency noticed after 5 cycles is maintained during further cycling the number of cycles was increased to ten. The results are shown in Fig. 5. Fig. 5 (a) reveals the occurrence of a local stress maxima during loading, suggesting the existence of a critical stress which must be overcome, from the 5th to the 10th cycle, in order that the deformation to proceed. On the other hand, Fig. 5 (b) reveals that no obvious changes occurred in stress variation during heating-cooling, excepting for the gradual increase of minimum stress.

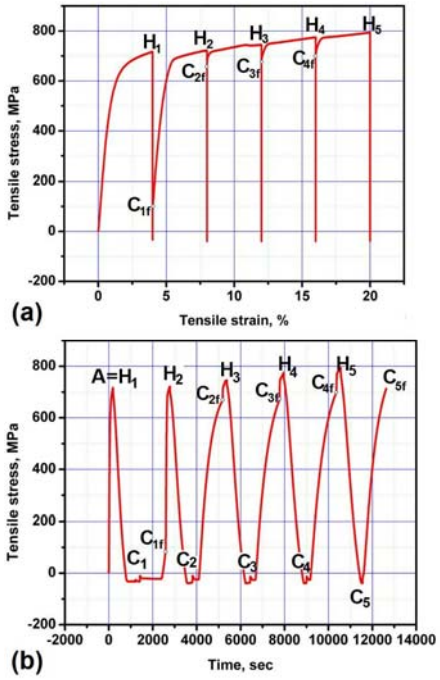

Fig. 4 Tensile constrained recovery behaviour during five cycles: (a) stress-strain curves; (b) stress variations in time during the entire cycling

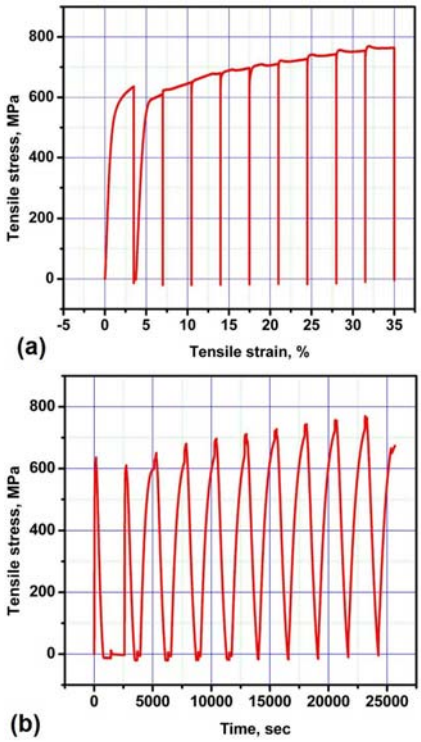

Fig. 5. Tensile constrained recovery behaviour during ten cycles: (a) stress-strain curves; (b) stress variations in time during the entire cycling.

A summary of the variation tendency of the maximum stress (σ) developed in Figs. 3-5 during cooling, with increasing the number of cycles (n), is shown in Fig. 6.

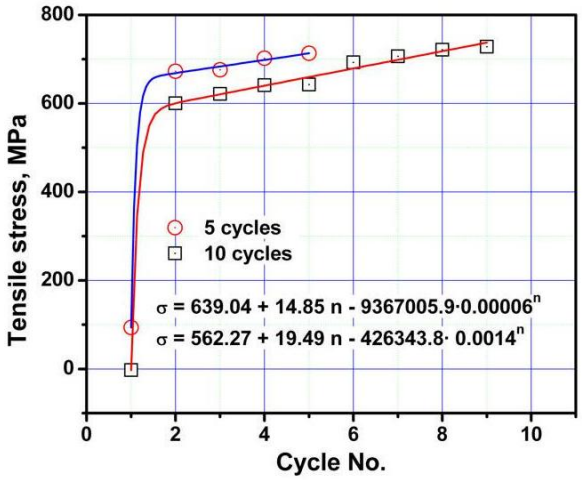

Fig. 6. The variation tendency of maximum stress developed during cooling, with increasing the number of cycles, can be fitted according to a Shah-type function.

Obviously, the variations of σ *vs.* n are fairly reproducible in the two series of cycles and fit Shah-type functions, according to the formula

$$\sigma = A + Bn + C\, r^n \qquad (3)$$

as illustrated in Fig. 6.

In order to correlate the change of recovery stress variation during cycling with microstructure evolution, Fig. 7 compares the SEM micrographs of initial and cycled states.

The microstructure revealed in Fig. 7 (a) is typical for fully recrystallized austenite, designated as γ-phase with face centred cubic (fcc) unit cell, observed after hot rolling and annealing of high chromium iron-manganese steels Due to the large amount of chromium, no ε (hcp) martensite is noticeable [13]. As an effect of annealing the hot rolled material, most of γ-phase grains are equiaxed and contain annealing twins (open triangles), which caused obvious relief variations. Due to recrystallization, no texturing tendencies are noticeable in γ-phase grains [14]. Moreover, some discrete marks of intercrystalline precipitation can be observed along γ-phase grain boundaries (illustrated with isolated red arrows) which suggests the presence of $(Fe, Mn)_3Si$ precipitates, as reported by Maji *et al*. [15].

The occurrence of stress-induced martensite, after 10 constrained recovery cycles, is noticeable in the SEM micrograph from Fig. 7 (b). This morphology is similar to that previously observed in low manganese Fe-Mn alloys, where it was considered that the presence of dissolved carbon acted as sites for heterogeneous nucleation, causing a reduction of martensite plate thickness [16], which is of the order of micrometers. As reported at a Fe-Mn-Si SMA, the stress induced martensite plates are also noticeable inside annealing twins (marked with open triangles) which generally deviated their direction [17]

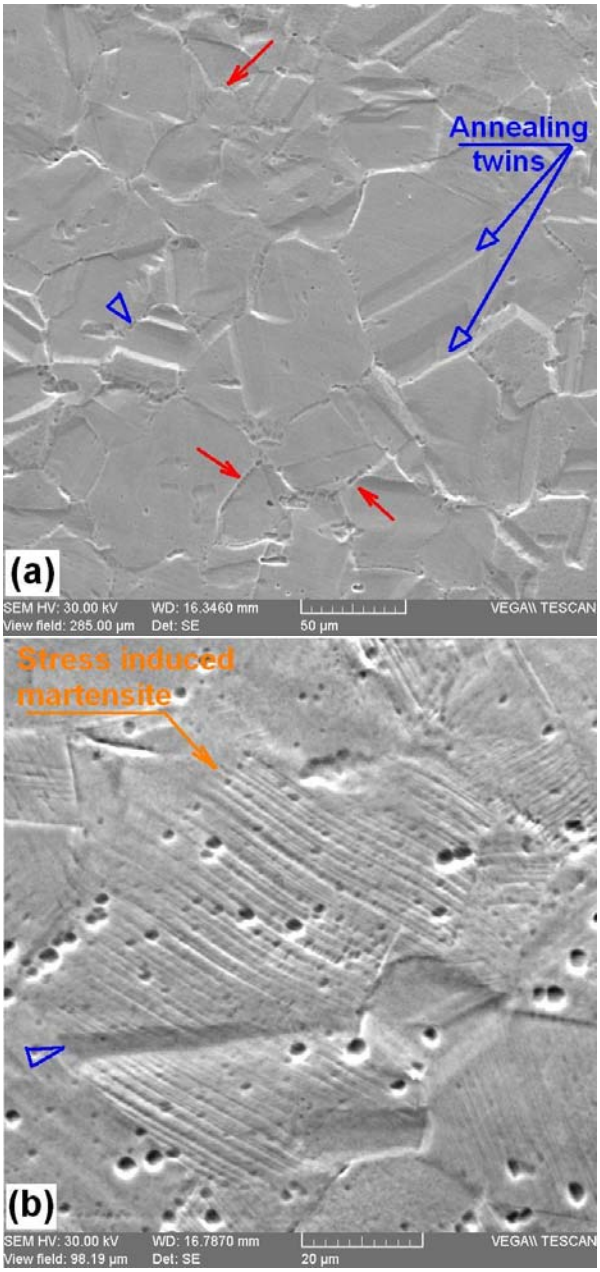

Fig. 7 Typical SEM micrographs of the gauges of tensile Fe-15.8 Mn-3.8 Si-12.3 Cr-4.7 Ni SMA specimens: (a) initial state, with fully austenitic structure, experiencing annealing twins (open triangles) and discrete intercrystalline precipitates (isolated arrows); (b) occurrence of stress induced martensite plates both inside γ-phase grains and inside annealing twins, after 10 constrained recovery cycles with a gradual strain increase of 3.5 % per cycle and heating cooling between RT and 453 K, observed on the specimen shown in the lower part of Fig. 2.

For a better observation of stress induced martensite plates, the surface relief was measured by SEM device, by

transforming luminescence fluctuations into depths variation, as shown in the inset of Fig. 8.

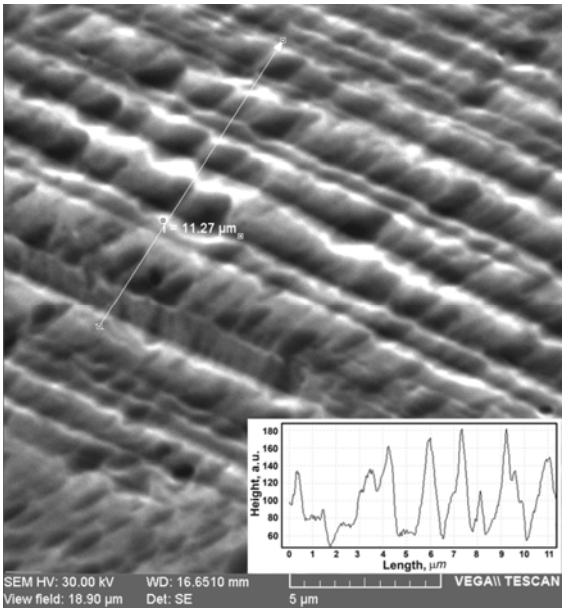

Fig. 8. Typical SEM micrograph of stress induced martensite plates formed after 10 constrained recovery cycles. The inset displays surface relief corresponding to the fiduciary line shown in the micrograph.

Fig. 8 illustrates a micrograph typical for stress induced martensite in low-carbon Fe-Mn-Si-Cr-Ni SMAs [18]. The surface relief shown in the inset evaluates the width of martensite plates to about 1×10^{-6} m and reveals the fact that no sub-plates are noticeable, since the plate walls are rather smooth.

4. Conclusions

The capacity on an Fe-15.8 Mn-3.8 Si-12.3 Cr-4.7 Ni SMA to be trained, during tensile constrained recovery cycles, has been revealed by means of the following variation tendencies: (i) increase of stress variation response when switching from heating to cooling; (ii) increase of minimum stress level from negative values to zero; (iii) slight increase with saturation tendency of the stress developed during cooling, which can fit a Shah-type function.

After 10 constrained recovery cycles, performed by heating-cooling at constant elongation, which continuously increased per each cycle, strains as high as 35 % were reached, characteristic to stress levels between 750-800MPa, which were accompanied by the formation of stress induced martensite plates.

The martensite plates, with typical thickness of the order of micrometers have been present even inside annealing twins and did not reveal any obvious substructure at micrometer level.

Acknowledgments

This work was supported by CNCSIS –UEFISCSU, project number PNII – IDEI code 301/ 2007. The support of Prof. S.Stanciu, in casting raw specimens, is gratefully acknowledged.

References

[1] L.-G. Bujoreanu, Materiale Inteligente, Editura Junimea, Iaşi, 117, 2002.
[2] J. L. Proft, T. W. Duerig, in Engineering Aspects of Shape Memory Alloys, (T. W. Duerig, K. N. Melton, D. Stöckel, C. M. Wayman, eds.), Butterworth-Heinemann, 115, 1990.
[3] S. Kajiwara, A. L. Baruj, T. Kikuchi, N. Shinya, Proc. of SPIE **5053**, 251 (2003).
[4] T. Maruyama, T. Kurita, S. Kozaki, K. Andou, S. Farjami, H. Kubo, Mater. Sci. Technol. **16,** 612 (2000).
[5] T. Sawaguchi, T. Kikuchi, K. Ogawa, S. Kajiwara, Y. Ikeo, M. Kojima, T. Ogawa, Mater. Trans. **47**(3) 580 (2006).
[6] Z. Z. Dong, S. Kajiwara, T. Kikuchi, T. Sawaguchi, Acta Mater. **53,** 4009 (2005).
[7] Y. Moriya, H. Kimura, S. Ishizaki, S. Hashizume, S. Suzuki, H. Suzuki, T. Sampei, J Phys **III**,.**1**, C4 (1991).
[8] N. Van Caenegem, L. Duperez, K. Verbeken, D. Degers, Y. Houbaert, Mater. Sci. Eng. A **481-482** 183 (2008).
[9] L. G. Bujoreanu, V. Dia, S. Stanciu, M. Susan, C. Baciu, Eur. Phys. J. Special Topics **158**, 15 (2008).
[10] L. G. Bujoreanu, S. Stanciu, R. I. Comăneci, M. Meyer, V. Dia, C. Lohan, J. Mater. Eng Perform. **18**, 500 (2009).
[11] L. G. Bujoreanu, S. Stanciu, B. Özkal, R. I. Comăneci, M. Meyer, ESOMAT 2009, 05003 (2009).
[12] J. C. Li, M. Zhao, Q. Jiang, Metall. Mater. Trans. A **31**, 581 (2000).
[13] L. Bracke, G. Mertens, J. Penning, B. C. De Cooman, M. Liebherr, N. Akdut, Metall. Mater. Trans. A **37**, 307 (2006).
[14] B. C. Maji, M. Krishnan, V. Hiwarkar, I. Samajdar, R. K. Ray, J Mater. Eng Perform. **18**, 588 (2009).
[15] B. C. Maji, M. Krishnan, V. V. Rama Rao, Metall. Mater. Trans. A **34**, 1029 (2003).
[16] T. Sawaguchi, L. G. Bujoreanu, T. Kikuchi, K. Ogawa, F. Yin, ISIJ Int. **48**(1), 99 (2008).
[17] T. Sawaguchi, L.-G. Bujoreanu, T. Kikuchi, K. Ogawa, M. Koyama, M. Murakami, Scripta Mater. 59, **826** (2008).
[18] K. M. Mostafa, J. De Baedemaeker, N. Van Caenegem, D. Degers, Y. Houbaert, J. Mater. Eng Perform. **18**, 575 (2009).

*Corresponding author: lgbujor@tuiasi.ro